Microporous and Mesoporous Materials 201 (2015) 234–239

Contents lists available at ScienceDirect

Microporous and Mesoporous Materials

journal homepage: www.elsevier.com/locate/micromeso

Mapping nanocavities in plugged SBA-15 with confined silver nanostructures

Rafael L. Oliveira, Mozaffar Shakeri, Johannes D. Meeldijk, Krijn P. de Jong, Petra E. de Jongh *

Inorganic Chemistry and Catalysis, Debye Institute for Nanomaterials Science, Utrecht University, The Netherlands

ARTICLE INFO

Article history:
Received 30 April 2014
Received in revised form 28 July 2014
Accepted 8 September 2014
Available online 19 September 2014

Keywords:
Plugged SBA-15
PHTS
Silver wires
Hard template synthesis

ABSTRACT

Silver nanostructures inside the pores of SBA-15 and plugged SBA-15 were synthesized and imaged, providing for the first time quantitative information about the nanocavity dimensions and plug distributions in plugged SBA-15.

1. Introduction

The synthesis of ordered mesoporous materials (OMM) has received much attention in the last two decades [1]. OMM have large surface areas, uniform pore sizes and tunable periodic pore arrangements. These properties make them attractive for applications in various fields such as catalysis, adsorption and drug delivery [2]. SBA-15 is the most studied mesoporous silica, because of its facile synthesis and stability.

In 2002, a new type of SBA-15 was reported and named plugged hexagonal templated silica (PHTS) or plugged SBA-15 [3]. These materials are synthesized using an excess of tetraethyl orthosilicate (TEOS), the silica precursor, leading to an ordered mesoporous silica with constricted pores [4]. By varying the synthesis parameters, the extent of the plugging can be influenced producing materials in which either all pores contain plugs ("completely plugged") or only a fraction of the pores contains plugs ("partially plugged"). In the case of PHTS materials the plugging is apparent from an ink bottle hysteresis in the N_2 physisorption isotherm, as liquid N_2 remains trapped by the narrow (plugged) entrances to the pores, resulting in delayed desorption. Moreover, these solids exhibit a remarkable mechanical and hydrothermal stability. In recent years, alternative strategies to produce PHTS materials have been proposed using different silica precursors and procedures [5].

Despite the importance of PHTS materials, the exact details of their structure have remained elusive. Van der Voort et al. proposed that the cylindrical SBA-15 channels were fully plugged, and only accessible via micropores in the channel walls [3]. On the other hand, Ryoo et al. explained the characteristics by an appreciable mesopore surface corrugation, possibly related to incomplete formation of plugs [6]. Zhao et al. pointed out that these solids just have a fraction of ordered mesopores exhibiting porous plugs within SBA-15 mesochannels [7].

In general, N_2 physisorption has been used to characterize porosity. Information about the size of the pores can be obtained from the adsorption branch and the accessibility of the pores (entrance sizes) can be derived from the desorption branch of the isotherm. However, the limitation is that only entrance sizes larger than ~4.7 nm can be characterized [8]. For plugged SBA-15 it is generally found that the entrance size is smaller than this limit. Argon at 77 K is an alternative as the capillary evaporation of argon at 77 K happens at lower relative pressures extending its use to analyze a wider range of constrictions in the porous structure, limited to entrance sizes larger than ~3.6 nm [9].

Other techniques such as electron tomography [10], modification of the silica surface using organosilanes [11] and metal oxide impregnation [12] have also been used to study these solids. However, none of these techniques is able to measure and quantify the nature of the plugging of the PHTS. A promising option is the use of replicas which are produced by filling the mesoporous structure with a carbon or a metal precursor (Au, Pt, Pd and others) followed by thermal treatment and silica removal [13]. This technique has been used to study the entrance size of 3-D mesoporous silica,

* Corresponding author at: Universiteitweg 99, 3584 CG Utrecht, The Netherlands. Tel.: +31 6 227 36 345; fax: +31 30 251 1027.
E-mail address: p.e.dejongh@uu.nl (P.E. de Jongh).

http://dx.doi.org/10.1016/j.micromeso.2014.09.026
1387-1811/

for example FDU-12 [14], and to identify the connections between pores in SBA-15 [15].

In this contribution, we present for the first time a study of the spatial distribution of the plugs, the dimensions and accessibility of the nanocavities in PHTS by synthesizing and imaging silver nanostructures confined inside the porous structure using TEM analysis.

2. Experimental section

2.1. Ordered-mesopore silica synthesis and silver deposition

2.1.1. Synthesis of the SBA-15

SBA-15 was synthesized following a procedure previously described [16]. In a polypropylene bottle 250 ml, 2.0 g of P123 blockcopolymer was dissolved in a mixture of 15 g of water and 60 g of 2 M HCl. This solution was stirred at 35 °C overnight. Then, 4.0 g of TEOS was added dropwise to this solution under vigorous stirring. After 5 min of stirring, the mixture was kept under static conditions at 35 °C for 20 h followed by 24 h at 80 °C. The solid product was collected by filtration, washed with distilled water, dried at 60 °C during 48 h and calcined at 550 °C in static air during 6 h.

2.1.2. Synthesis of the PHTS materials

Samples were designated PHTS-A-B, A indicating in how many steps TEOS was added and B indicating the hydrothermal treatment temperature.

2.1.3. PHTS-1-60, PHTS-1-80, PHTS-1-100

In a polypropylene bottle 250 ml, 2.0 g of P123 blockcopolymer was dissolved in a mixture of 15 g of water and 60 g of 2 M HCl. This solution was stirred at 35 °C overnight. Then, 8.5 g of TEOS was added dropwise during 15 min to this solution under vigorous stirring. After 5 min of stirring, the mixture was kept under static condition at 35 °C for 20 h followed by 24 h at different temperature (60, 80 and 100 °C). The solid product was collected by centrifugation, washed with distilled water, dried at 60 °C during 48 h and calcined at 550 °C in static air during 6 h.

2.1.4. Synthesis of the PHTS-2-80

In a polypropylene bottle 250 ml, 2.0 g of P123 blockcopolymer was dissolved in a mixture of 15 g of water and 60 g of 2 M HCl. Then, 4.25 g of TEOS was added to this solution under vigorous stirring. The solution was kept stirring for 30 min, then, 4.25 g of TEOS was added dropwise in this solution. The mixture was kept under static condition at 35 °C for 20 h followed by 24 h at 80 °C. The solid product was collected by centrifugation, washed with distilled water, dried at 60 °C during 48 h and calcined at 550 °C in static air during 6 h.

2.1.5. Deposition of the silver nanowires

Silver structures on SBA-15 were synthesized using using a two-solvent technique [17]. In this methodology, 300 mg of mesoporous silica was first dried at 120 °C for 12 h to remove physisorbed water. Then, 5 ml of n-hexane was added to the dried mesoporous silica and this suspension was stirred vigorously during 10 min.

After this procedure, 2 ml of 1.25 M $AgNO_3$ aqueous solution was added to this suspension dropwise. Then, the suspension was stirred during 4 h at room temperature, the composite was centrifuged, dried at 80 °C for 6 h to remove n-hexane and then heated to 350 °C with a temperature increase rate of 2 °C/min, and calcined at 350 °C in stagnant air during 2 h.

The synthesis of Ag-PHTS-1-60 with a lower metal loading was done using exactly the same procedure described above, but changing the volume of the silver nitrate solution (1 ml). The metal loadings were determined by AAS (Mikroanalytisches Laboratorium Kolbe, Germany).

Freestanding silver nanowires were obtained by dissolving the SBA-15. In this procedure, 50 mg of Ag-SBA-15 was added to a solution of 3.0 M of NaOH (1.0 ml), then, this mixture was stirred during 24 h. After this period, the silver wires were retrieved by centrifugation and washed with distillated water and ethanol.

2.2. Structural analysis

2.2.1. XRD analysis

Long range pore ordering was confirmed with low-angle X-ray diffraction. Patterns were obtained at room temperature from 0.5 to 8° 2θ with a -AXS D2 Phaser powder X-ray diffractometer, in Bragg–Brentano mode, equipped with a Lynxeye detector using Co–$K_{\alpha 12}$ radiation, with λ = 1.790 Å, operated at 30 kV, 10 mA. To provide reproducible results and minimize effects of sample preparation the average over three individual small angle XRD measurements was used. XRD patterns of silver were recorded for all solids between 10 and 100° 2θ using the same equipment.

2.2.2. N_2 and Ar physisorption

N_2 and Ar physisorption measurements were performed at 77 K using a Micromeritics Tristar 3000. The samples were dried before the measurement under an N_2 flow at 250 °C for at least 12 h. The total microporous and mesoporous volume (V_p) was determined using the *t*-plot method. The pore size distribution of the mesoporous silica supports was calculated from the adsorption branch of the isotherm by BJH analysis. The maximum of the pore size distribution was taken as the average pore diameter. The percentage of plugged mesopore volume that was calculated from the cumulative pore volume as a function of the pore size distribution (BJH analysis of the desorption branch) by defining the peak as 3.5–4.0 nm as plugged pores (more details Supporting information S2).

2.2.3. Quantification of plugged (SEM and TEM analysis)

The morphology and sizes of the silica particles were determined with a Tecnai FEI XL 30SFEG Scanning Electron Microscope (SEM). Transmission electron microscopy was performed using a microscope FEI Tecnai 20F, operated at 200 kV equipped with CCD camera.

The samples were embedded in epoxy resin (Epofix, EMS) and cured at 60 °C overnight. Then, they were cut into thin sections with a nominal thickness of 60 nm using a Diatome Ultra knife, 4 mm wide and 35° clearance angle, mounted on a Reichert–Jung Ultracut E microtome. The sections float on water after cutting, were picked up and deposited onto a carbon coated polymer grid and left to dry.

The histograms of particle size distribution were obtained from observing about 500 particles in representative micrographs of different areas.

3. Results and discussion

3.1. PHTS structure

The small-angle powder XRD patterns of PHTS (Supporting information S3) shows three diffraction peaks that can be assigned to the (100), (110) and (200) planes, corresponding to a hexagonal *p6mm* arrangement of the pores. The peaks have lower intensities for PHTS than for SBA-15. This can be explained by the presence of plugs inside the pores, which decrease the difference in electron density between pores and silica walls. SEM (Supporting information S4) showed that the plugged SBA-15 particles have

a uniform morphology with sizes of 1–2 μm and the shape of the particles was affected slightly by the hydrothermal synthesis temperatures. TEM analysis (Fig. 1) faced the pore structure of PHTS materials. It is possible to observe that increasing the hydrothermal temperature the pores became larger. HAADF-STEM was also used to study the PHTS-1-60 showing the constrictions inside the pore structure of this material (Supporting information S5).

Nitrogen isotherms at 77 K are shown in Fig. 2 (top frame). The isotherms show hysteresis in the pressure range of $p/p_0 = 0.4–0.8$ indicative of the presence of mesopores. N_2 physisorption isotherms of samples PHTS-2-80 and PHTS-1-100 show a 2-steps desorption. The first desorption step is due to desorption from open mesopores. The second desorption step is attributed to plugged mesopores and used to calculate the fraction of plugged mesopore volume. Comparison of results for PHTS-2-80 and PHTS-1-80 shows that adding the silica precursor in two steps leads to only partially plugged materials (2-steps desorption); however, slow addition in one step resulted in completely plugged SBA-15 (1-step desorption) (extra explanation on Supporting information S1). All N_2 desorption isotherms showed cavitation at ~0.42 relative pressure, indicating that the entrance size of some plugged mesopores is smaller than 4.7 nm.

Ar physisorption (Fig. 2, bottom frame) allows extending this measurement limit down to ~3.6 nm.[18] In the case of PHTS-1-80 and PHTS-2-80, Ar physisorption (Fig. 2 bottom frame) displays a continuous gas desorption at relative pressures from 0.6 to 0.35, showing that constrictions inside the mesopores had a broad size distribution with entrance sizes from 5.6 to 3.6 nm. Thus, the PHTS-1-80 materials are accessible through mesosized entrances and not only through micropores as reported earlier [3]. For PHTS-1-60 1-step desorption was observed again, facing smaller entrance sizes which are not able to be measured by argon physisorption.

Table 1 provides an overview of the structural properties of the materials. If the aging temperature is raised from 60 to 100 °C, the unit cell parameter increases from 9.0 to 10.7 nm, while also the pore diameter and total pore volume increase. In general, the accessibility of the mesopores is related to the mesopore diameter. The sample PHTS-1-60, which has mesopores of ~4.5 nm, is only accessible through entrances smaller than 3.6 nm. The samples PHTS-1-80, PHTS-1-100 and PHTS-2-80 (pore diameter 6.0, 7 and 6.7 nm respectively) have partially open mesopores and larger window sizes. The micropore volume is low when the hydrothermal temperature was 100 °C. It has been well documented for SBA-15 that the micropores are related to the hydrophilic nature of the PEO chains of the organic template around which silica is grown and that at 100 °C, the PEO blocks become less hydrophilic, leading to lower micropore volumes [19].

3.2. Silver deposition

Although gas physisorption gives information about the average properties of the samples, such as surface area and plugged porosity, it does not show where the plugs and cavities are located inside the material. Thus, to gain a better understanding of spatial distribution of constrictions and cavities in these solids, silver structures were synthesized inside the mesopores of silica, giving local information about the pore structure of these materials. Moreover, samples with different silver loadings were synthesized to verify that the use of relatively low silver volume loadings, as used in this study, did not lead to preferential silver deposition in certain mesopores.

Fig. 3 shows TEM images of SBA-15 material containing silver nanowires (frame A and B) and silver nanowires obtained after silica removal (frame C). Very long silver nanowires running over the full length of the silica particles are observed (Fig. 3A), confirming

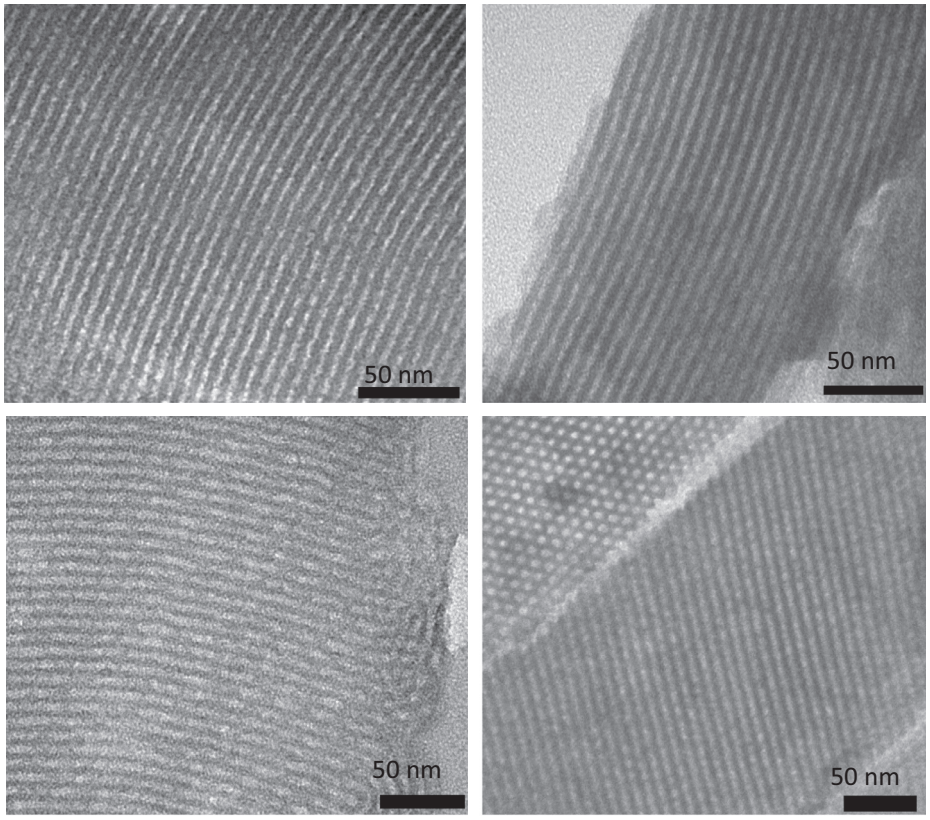

Fig. 1. TEM images: PHTS-1-60 (top-left), PHTS-2-80 (top-right), PHTS-1-80 (bottom-left), PHTS-1-100 (bottom-right).

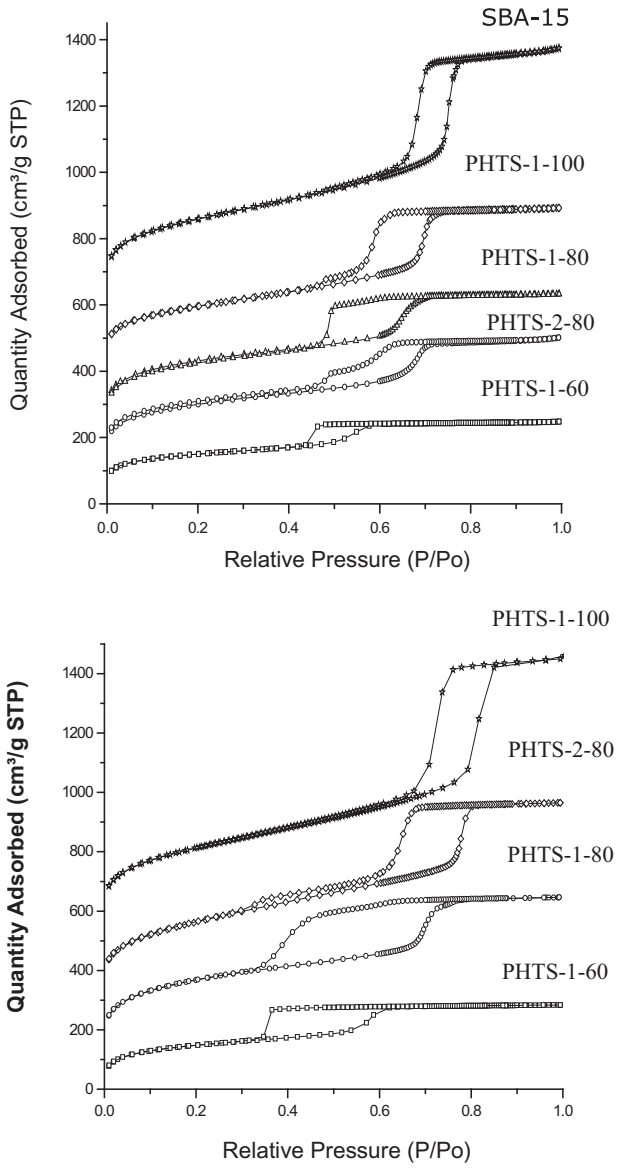

Fig. 2. N_2 physisorption (top frame) and Ar physisorption (bottom frame) measured at 77 K. The N_2 isotherms were offset vertically by 100, 200, 400, 600 cm^3/g STP; Ar physisorption isotherms for PHTS were offset vertically 100, 200, 500 cm^3/g STP.

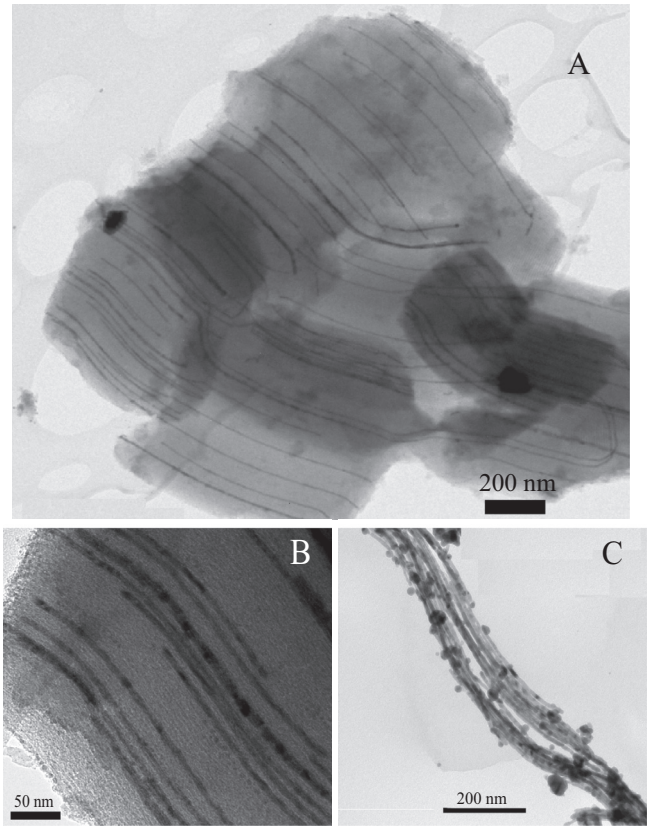

Fig. 3. Silver nanowires inside SBA-15 (A, B), silver nanowires after silica removal (C).

the regular open mesopore structure of SBA-15. The Ag nanowires were around 7.2 nm in diameter (Fig. 3B), in accordance with the pore diameter of SBA-15. Despite the pore corrugation of SBA-15 that has been reported before [10], the silver nanowires have not broken up into smaller rods (Fig. 3A). Part of the pores was filled completely, while other pores contain no Ag, which is not unexpected given the fact that after drying the silver nitrate corresponds to 20% of the pore volume, while conversion to silver results in another 10% volume decrease. Moreover, the redistribution of mobile intermediate phases during the thermal treatment can also explain the distribution of silver in SBA-15, as has been observed before for Ni, Co and other metals [20]. N_2 physisorption of Ag-SBA-15 confirmed a reduction of total pore volume and the absence of cavities after silver formation (Fig. S6, Supporting information). Furthermore after silica removal, long silver wires were obtained (frame 2C). The stability of these wires was limited, which might be due to electron beam exposure. Nevertheless, it is clear that the silver nanostructures faithfully represent the pore structure of the SBA-15 material. Hence based on this result, we decided to probe the nanocavities and pore constrictions in PHTS by imaging silver nanorods grown in the pores.

Ag-PHTS-2-80 (Fig. 4) showed clearly shorter silver structures than Ag-SBA-15. Silver rods of 70–100 nm length were observed, showing that in some pores the distance between the constrictions was relatively long (Fig. 4A). In other areas of the sample even shorter silver rods with 15–30 nm of length were observed, indicating even shorter distances between the constrictions

Table 1
Structural properties of samples as derived from N_2 physisorption and XRD.

Sample	a_o (nm)	d (nm)	S_{BET} (m^2/g)	V_{total} (cm^3/g)	V_{meso} plugged (%)	V_{micr} (cm^3/g)
SBA-15	10.7	7.0	917	1.18	0	0.06
PHTS-1-60	9.0	4.5	508	0.38	100	0.10
PHTS-1-80	10.2	6.0	797	0.67	96	0.11
PHTS-1-100	10.7	7.0	694	0.76	19	0.05
PHTS-2-80	10.7	6.5	695	0.61	41	0.08

a = lattice spacing, d = pore diameter from adsorption branch (BJH), S_{BET} = BET surface area, V_{total} = total pore volume, V_{meso} plugged = volume of plugged mesopores, V_{micro} = micropore volume.

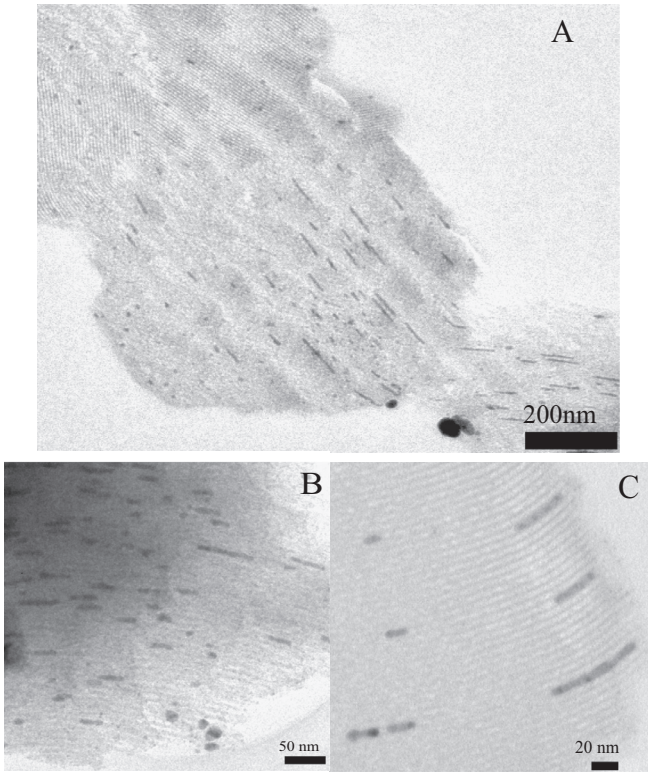

Fig. 4. Silver nanowires and nanorods inside PHTS-2-80.

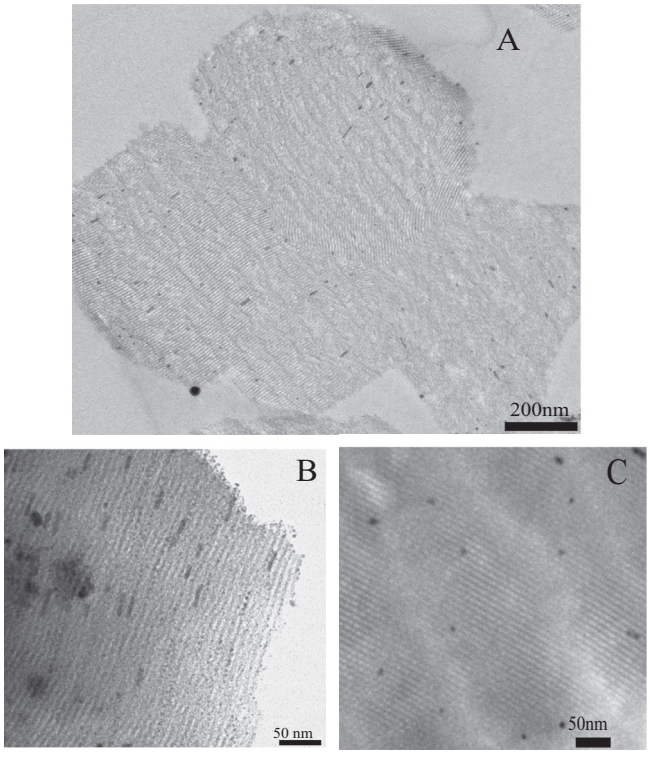

Fig. 6. Silver nanorods inside PHTS-1-80 (top, bottom left) PHTS-1-60 (bottom right).

(Fig. 4A–C). A histogram (Fig. 5A) confirms a wide distribution of silver structures inside PHTS-2-80. The relatively large distances between the plugs are in accordance with the physisorption which shows 41% of mesopore volume contains plugs. Since in PHTS the nanorods are short in contrast to those in SBA-15 we conclude that in PHTS materials the constrictions are narrow enough to stop the continuous growth of the silver wires.

Samples Ag-PHTS-1-60 and Ag-PHTS-1-80 contain much shorter silver nanorods, mainly around 10–40 nm of length, and even silver nanoparticles (Fig. 6).The length of the rods is nicely in line with direct imaging of cavities (Fig. S3). Frame A illustrates that for Ag-PHTS-1-80 plugs with small inter-plug distances are abundant throughout the whole material. The average rod length was 28 ± 7.5 nm (Fig. 5B). For Ag-PHTS-1-60, with the smallest pores, some silver deposits were observed outside the silica structure (Fig. S8). Inside the mesoporous structure only spherical particles and short rods are observed (Fig. 6C) illustrating the severe constriction of all pores. These results are in accordance with gas physisorption results which showed that PHTS-1-60 and PHTS-1-80 have 100% and 96% of their mesopore volume plugged, respectively. PHTS-1-60 was prepared with different silver loadings (20 and 35 w/w% Fig. S9). No influence of the silver loading on the length distribution of the rods was observed. This result differs from that obtained by Wang et al. [21] who observed an influence of the metal loading of Au, Ag and Pt in SBA-15 on the particle size. This fact gives a strong indication that in our case imaging the Ag plugs inside the PHTS materials faithfully represents the mesopore structure.

4. Conclusions

Visualizing silver nanostructures confined in the pores of SBA-15 and plugged SBA-15 allows a detailed characterization of the porosity in these materials. For SBA-15, Ag nanowires extended over the full pore length. Plugged SBA-15 materials were prepared with a variation in the degree of constriction of the pores. Especially a lower hydrothermal treatment temperature resulted in a

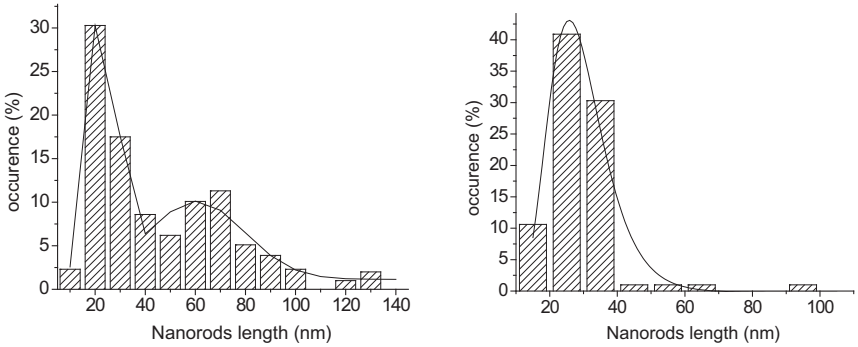

Fig. 5. Length distribution of Ag nanorods in PHTS-2-80(left), and PHTS-1-80(right).

higher degree of plugging, with virtually all pores containing plugs. The length of the enclosed nanocavities was determined, and varied from 10 to 100 nm, depending on the synthesis procedure. These results demonstrate the suitability of visualization of pore-confined metal nanostructures to characterize the nature of complex porosities such as in nanocavities-containing materials.

Acknowledgments

The authors thank the Dutch National Research School Combination Catalysis Controlled by Chemical Design (NRSC-Catalysis) for the financial supporting and Marjan Versluijs-Helder for the SEM analysis.

Appendix A. Supplementary data

Supplementary data associated with this article can be found, in the online version, at http://dx.doi.org/10.1016/j.micromeso.2014.09.026.

References

[1] V. Meynen, P. Cool, E.F. Vansant, Micropor. Mesopor. Mater. 125 (2009) 170–223.
[2] (a) M. Shakeri, R.J.M. Klein Gebbink, P.E. de Jongh, K.P. de Jong, Angew. Chem. Int. Ed. 52 (2013) 1–5;
(b) J. Sun, X. Bao, Chem. Eur. J. 14 (2008) 7478–7488;
(c) B.J. Melde, B.J. Johnson, P.T. Charles, Sensors 8 (2008) 5202–5228;
(d) I.I. Slowing, J.L. Vivero-Escoto, C.W. Wu, V.S.-Y. Lin, Adv. Drug Deliv. Rev. 60 (2008) 1278–1288;
(e) L.P. Mercuri, L.V. Carvalho, F.A. Lima, C. Quayle, M.C.A. Fantini, G.S. Tanaka, W.H. Cabrera, M.F.D. Furtado, D.V. Tambourgi, J.R. Matos, M. Jaroniec, O.A. Sant'Anna, Small 2 (2006) 254–256.
[3] P.V.D. Voort, P.I. Ravikovitch, K.P. De Jong, M. Benjelloun, E.V. Bavel, A.H. Janssen, A.V. Neimark, B.M. Weckhuysen, E.F. Vansant, J. Phys. Chem. B 106 (2002) 5873–5877.
[4] (a) E.V. Bavel, P. Cool, K. Aerts, E.F. Vansant, J. Phys. Chem. B 108 (2004) 5263–5268;
(b) M. Mandal, M. Kruk, Chem. Mater. 24 (2011) 149–154.
[5] (a) W. Wang, W. Shan, H. Ru, J. Mater. Chem. 21 (2011) 17433–17440;
(b) J. Lee, Y. Park, Pil Kim, H. Kim, J. Yi, J. Mater. Chem. 14 (2004) 1050–1056;
(c) B.-H. Min, E.-Y. Jeong, M. Thommes, S.-E. Park, Chem. Commun. 47 (2011) 4673–4675;
(d) E.V. Bavel, P. Cool, K. Aerts, E.F. Vansant, J. Porous Mater. 12 (2005) 65–69.
[6] M. Kruk, M. Jaroniec, S.H. Joo, R. Ryoo, J. Phys. Chem. B 107 (2003) 2205–2213.
[7] Y. Wan, D. Zhao, Chem. Rev. 107 (2007) 2821–2860.
[8] J.C. Groen, J. Pérez-Ramírez, Appl. Catal. A Gen. 268 (2004) 121–125.
[9] M. Kruk, M. Jaroniec, Chem. Mater. 13 (2001) 3169–3183.
[10] (a) A.H. Jansen, P.V.D. Voort, A.J. Koster, K.P. De Jong, Chem. Commun. (2002) 1632–1633;
(b) C.J. Gommes, H. Friedrich, M. Wolters, P.E. de Jongh, K.P. de Jong, Chem. Mater. 21 (2009) 1311–1317.
[11] M. Shakeri, R.J.M. Klein Gebbink, P.E. de Jongh, K.P. de Jong, Micropor. Mesopor. Mater. 170 (2013) 340–345.
[12] V. Meynen, Y. Segura, M. Mertens, P. Cool, E.F. Vansant, Micropor. Mesopor. Mater. 85 (2005) 119–128.
[13] M. Tiemann, Chem. Mater. 20 (2008) 961–971;
M. Worboys, P.P. Edwards, P.A. Anderson, Chem. Commun. (2002) 2894–2895;
H.J. Shin, R. Ryoo, M. Kruk, M. Jaroniec, Chem. Commun. (2001) 349–350;
M.H. Huang, A. Choudrey, P. Yang, Chem. Commun. (2000) 1063–1064;
Y.-J. Han, J.M. Kim, G.D. Stucky, Chem. Mater. 12 (2000) 2068–2069.
[14] J. Fan, C. Yu, F. Gao, J. Lei, B. Tian, L. Wang, Q. Luo, B. Tu, W. Zhou, D. Zhao, Angew. Chem. Int. Ed. 42 (2003) 3146–3150.
[15] R. Ryoo, C.H. Ko, M. Kruk, V. Antochshuk, M. Jaroniec, J. Phys. Chem. B 104 (2000) 11465–11471.
[16] A. Sayari, B.H. Han, Y. Yang, J. Am. Chem. Soc. 126 (2004) 14348–14349.
[17] X. Huang, W. Dong, G. Wang, M. Yang, L. Tan, Y. Feng, X. Zhang, J. Colloid Interface Sci. 359 (2011) 40–46;
J. van der Meer, I.B. Giboire, C. Mercnier, B. Revel, A. Davidson, R. Denoyel, J. Phys. Chem. C 114 (2010) 3507–3515.
[18] T.M. Eggenhuisen, J. Zecevic, H. Talsma, K.P. de Jong, P.E. de Jongh, J. Phys. Chem. C 116 (2012) 7480–7490.
[19] P.F. Fulvio, S. Pikus, M. Jaroniec, J. Mater. Chem. 15 (2005) 5049–5053.
[20] (a) J.R.A. Sietsma, J.D. Meeldijk, J.P. Den Breejen, M. Versluijs-Helder, A.J. van Dillen, P.E. de Jongh, K.P. de Jong, Angew. Chem. Int. Ed. 46 (2007) 4547–4549;
(b) R.L. Oliveira, P.K. Kiyohara, L.M. Rossi, Green Chem. 12 (2010) 144–149.
[21] Z. Wang, Y. Xie, C. Liu, J. Phys. Chem. C 112 (2008) 19818–19824.